INVESTIGATION OF SOFT ELASTOMERIC CAPACITOR FOR THE MONITORING OF LARGE ANGULAR MOTIONS

HAN LIU*, SIMON LAFLAMME†‡, SDIQ ANWAR TAHER§, JONG-HYUN JEONG**, JIAN LI§, CAROLINE BENNETT§, WILLIAM N. COLLINS§, DAVID J. EISENMANN††, AUSTIN DOWNEY‡‡§§, PAUL ZIEHL‡‡§§, AND HONGKI JO**

ABSTRACT

Angular motion measurement using commercial sensing technologies can be challenging due to the nonlinearity of the motion and the combination of translational, oscillatory, and rotational behaviors. Recent advances in hyperelastic and self-sensing materials have facilitated the development of flexible electronics, enabling robust and cost-effective angular motion sensing systems. The authors have recently proposed a flexible strain sensor termed corrugated soft elastomeric capacitor (cSEC). The cSEC is a thin-film, ultra-compliant, and scalable sensor that transduces geometric variations into a measurable change in capacitance. It is constituted by layering two conductive plates sandwiching a dielectric that is surface-corrugated. In this paper, we study the use of the cSEC for angular motion sensing of a free rotational hinge, in which the cSEC was adhered onto the rotating area of the hinge subjected to an axial displacement generating clockwise and counterclockwise angular rotations.

KEYWORDS: flexible strain gauge, angular motion sensing, bending strain, complex geometry, out-of-plane deformation, strain monitoring, structural health monitoring

Introduction

The angular motion of an object is widely defined as the combination of translational, oscillatory, and rotational motion (Davidovits 2018). The simultaneous detection and monitoring of angular motion plays a significant role in the determination of the deflective shape and permits estimation and diagnosis of engineering structures. For example, monitoring the angular motion at a weld could be used in estimating fatigue susceptibility and planning of maintenance actions. Conventional methods for angular motion sensing mainly rely on mechanical systems combined with various velocity and displacement transducers and reflective sensors (e.g., retro-reflective and photo-reflective sensors). They can be expensive, time-consuming, and labor-intensive to apply in the field (Algrain and Saniie 1991; Peña Arellano et al. 2013; Zhang and Menq 1999; Penning et al. 2005).

A solution is to use thin-film devices, which have recently gained popularity with advances in materials and flexible electronics. Numerous thin-film sensors have been proposed in literature in the form of flexible electronics based on capacitance (Guo et al. 2019; Yang et al. 2019), resistance (Mu et al. 2018; Shao et al. 2021), piezoelectrics/triboelectrics (Chowdhury et al. 2019; Liu, J. et al. 2021), and transistance (Viola et al. 2018; Wang et al. 2020) to measure strain (Qu et al. 2020; Sun et al. 2020), stress (Gao et al. 2019; Gowthaman et al. 2019), pressure (Tannarana et al. 2020; Yu et al. 2021), temperature (Liu, Q. et al. 2018; Liu, G. et al. 2019), and so on.

Compared to off-the-shelf sensors (e.g., optimal encoder, tiltmeters), a critical advantage of flexible sensors is in their mechanical compliance, which allows a deployment over complex and irregular geometries such as rugged surface, corners, and welds. Of interest here is the measurement of angular motion, where the sensor is allowed to fold along with the motion. Examples of such technologies include a graphene sensor fabricated by introducing liquid metal into microfluidic channels (Jiao et al. 2016), a soft-squishy sensor fabricated by embedding flexible wires in a silicone elastomer (Prituja et al. 2018), a graphene platelet (GnP) and multi-walled carbon nanotube (MWCNT)-based film strain sensor (Lu et al. 2019), a thin film created by arranging planar coils in a cylindrical pattern (Anandan et al. 2018), and a self-powered sensor fabricated by integrating a stack of magnets and coils into a flexible tube (Askari et al. 2018).

Our group has recently proposed a corrugated soft elastomeric capacitor (cSEC) that is a thin-film, flexible, and

* Department of Civil, Construction and Environmental Engineering, Iowa State University, Ames, IA, 50010, USA; liuhan@iastate.edu; 1-515-294-2140
† Department of Civil, Construction and Environmental Engineering, Iowa State University, Ames, IA, 50010, USA
‡ Department of Electrical and Computer Engineering, Iowa State University, Ames, IA, 50010, USA
§ Department of Civil, Environmental and Architectural Engineering, The University of Kansas, Lawrence, KS, 66045, USA
** Department of Civil, Architectural Engineering and Mechanics, The University of Arizona, Tucson, AZ, 85721, USA
†† Department of Agricultural and Biosystems Engineering, Iowa State University, Ames, IA, 50010, USA
‡‡ Department of Mechanical Engineering, University of South Carolina, Columbia, SC, 29208, USA
§§ Department of Civil and Environmental Engineering, University of South Carolina, Columbia, SC, 29208, USA

Materials Evaluation 81 (2): 46–51
https://doi.org/10.32548/2023.me-04294

ultra-compliant sensor creating a parallel plate capacitor through a corrugated dielectric layer sandwiched between two conductive plates (Liu, H. et al. 2020b). The cSEC is capable of transducing mechanical strain into a measurable change in capacitance. Prior work showed sensing signal linearity up to 40% strain, and demonstrated the technology for various applications including fatigue crack monitoring on structural steel component (Liu, H. et al. 2021a; 2021b), and stress evaluation in biological tissues (Liu, H. et al. 2020a; 2021c). Its dynamic behavior has been characterized up to 40 Hz (Laflamme et al. 2015).

In this paper, we investigate the use of the cSEC for measuring large angular motions. This is done by deploying the cSEC onto the rotating portion of a free rotational hinge subjected to angular rotation between 0° and ±60° in a static regime. An extended electromechanical model is proposed and verified using finite element model (FEM) and experimental data.

Background

This section provides a background on the textured SEC technology, followed by a derivation of an extended electromechanical model adopted for SEC's capacitance response under bending strain deformation.

Corrugated SEC Technology

The fabrication process along with the sensing principle of non-corrugated SEC is documented in detail in Laflamme et al. (2013), and that of the corrugated version (cSEC) in Liu et al. (2020b). Briefly, the dielectric of an SEC is fabricated using a styrene-co-ethylene-co-butylene-co-styrene (SEBS) block co-polymer matrix filled with PDMS-coated titania (TiO_2), and the conductive plates using the same SEBS matrix but filled with carbon black particles. The corrugated surface of the dielectric layer is created by drop-casting the SEBS composite solution into a grooved steel mold and peeling it off after drying, after which the electrode solution is painted onto both surfaces and allowed to dry. The electrical connections to the data acquisition system (DAQ) are created using copper tabs adhered onto the conductive layers. Figure 1a is a picture of a grid-patterned cSEC with a sensing area of 76 cm². The consistency and uniformity of the sensors is ensured through the measurement of geometric (e.g., material thickness at several points) and electrical (e.g., initial capacitance of the sensor, resistance of the electrodes) properties.

Electromechanical Model under Angular Motion

A particular feature of the cSEC is its ability to transduce strain into a measurable change in capacitance, which enables the measurement of additive in-plane strain (x-y plane in Figure 1b) under plane-stress. Assuming a low measurement frequency (< 1 kHz), the cSEC can be modeled as a non-lossy capacitor with the initial capacitance C_0 derived from a parallel plate capacitor:

$$(1) \quad C_0 = e_0 e_r \frac{A}{h}$$

where

e_0 = 8.854 pF/m is the vacuum permittivity,
e_r is the relative permittivity,
h is the thickness of the dielectric, and
A is the electrode area of length l and width w as annotated in Figure 1b.

To derive the electromechanical behavior under angular motion, consider a small unit of the cSEC of initial length l, width w, and thickness h, as shown in Figure 2a. The unit is assumed to be small enough such that strain is distributed uniformly. By applying a uniaxial stretch along the y-direction, the small unit deforms to length l', width w', and thickness h'. The relative change in capacitance ($\Delta C/C_0$) of the unit under deformation becomes:

$$(2) \quad \frac{\Delta C}{C_0} = \frac{C_1 - C_0}{C_0} = \frac{e_0 e_r\left(\frac{A'}{h'} - \frac{A}{h}\right)}{e_0 e_r \frac{A}{h}} = \frac{A'h - Ah'}{Ah'}$$

where

ΔC is the change in capacitance,
C_1 is the capacitance under deformation, and
$A = lw$ and $A' = l'w'$ are the initial and deformed electrode areas, respectively.

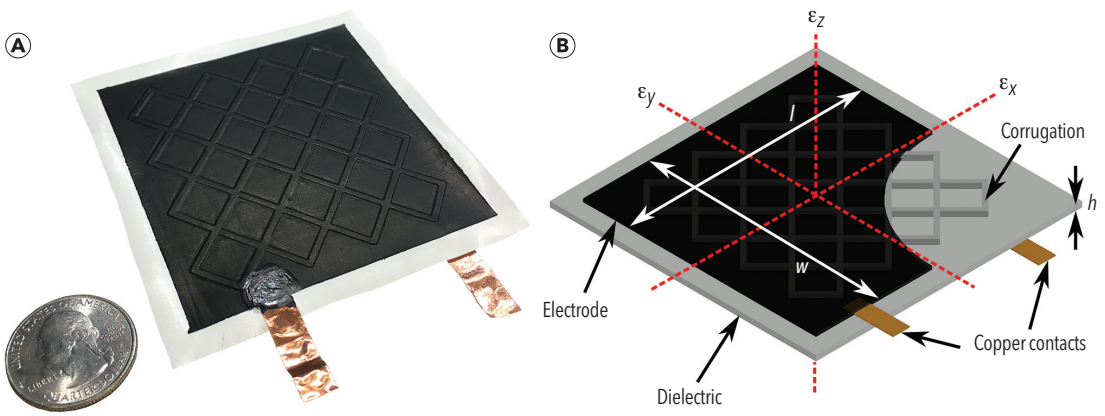

Figure 1. The corrugated soft elastomeric capacitor (cSEC): (a) picture of a 76 × 76 mm grid-patterned cSEC; and (b) schematic of thickness h and electrode area $l \times w$ (black layer).

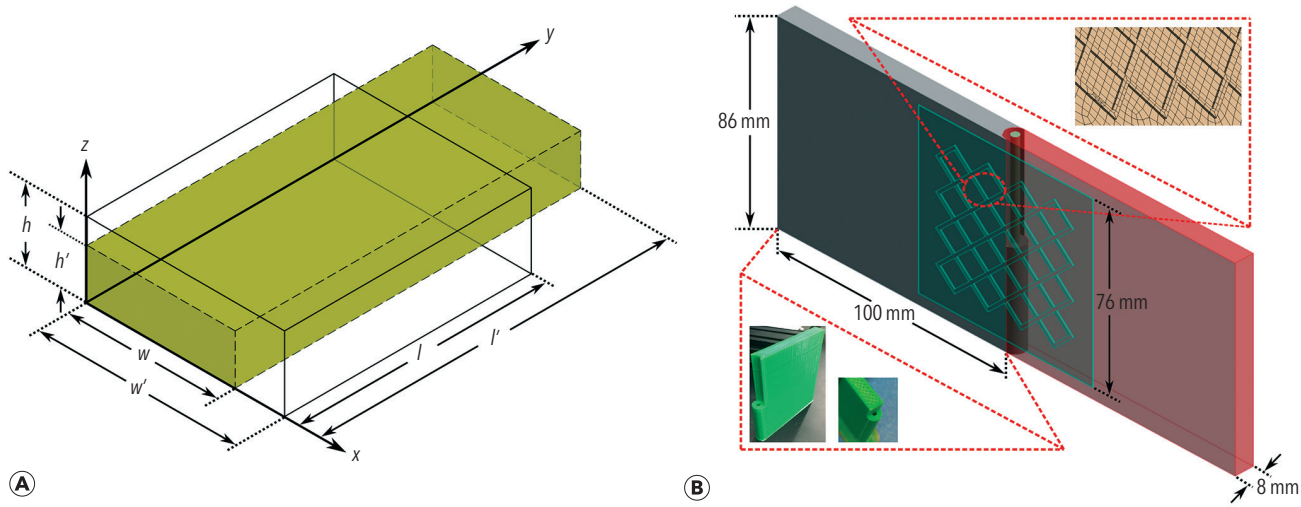

Figure 2. Schematics: (a) single mesh element of the sensor; (b) free rotational hinge with cSEC.

Substituting A and A' into Equation 2 yields:

$$(3)\quad \frac{\Delta C}{C_0} = \frac{l'w'h - lwh'}{lwh'}$$

Taking $l' = (1 + \varepsilon_x)l$, $w' = (1 + \varepsilon_y)w$, and $h' = (1 + \varepsilon_z)h$, Equation 3 becomes:

$$(4)\quad \frac{\Delta C}{C_0} = \frac{(1 + \varepsilon_x)(1 + \varepsilon_y)}{1 + \varepsilon_z} - 1$$

Using Hooke's Law and assuming plane stress with Poisson's ratio ν, the stress along the z-axis can be written as:

$$(5)\quad \varepsilon_z = -\frac{\nu}{E}(\sigma_x + \sigma_y) = -\frac{\nu}{1-\nu}(\varepsilon_x + \varepsilon_y) = \frac{1}{(1 + \varepsilon_x)(1 + \varepsilon_y)} - 1$$

Substituting Equation 5 into Equation 4 gives:

$$(6)\quad \frac{\Delta C}{C_0} = (1 + \varepsilon_x)^2(1 + \varepsilon_y)^2 - 1$$

Denoting $\nu_{xy} = -\frac{\varepsilon_y}{\varepsilon_x}$ as the transverse Poisson's ratio of the corrugated dielectric layer under a free-standing configuration, and ν_m as the Poisson's ratio of the monitored material, the Poisson's ratio under composite action, $\nu_{xy,c}$, assuming full adhesion to the monitored material, can be written:

$$(7)\quad \nu_{xy,c} = -\frac{a\nu_{xy} + b\nu_m}{a + b} = -\frac{\varepsilon_{y,c}}{\varepsilon_{x,c}}$$

where

a and b are the weights determined from the stiffness of materials, and

$\varepsilon_{x,c}$ and $\varepsilon_{y,c}$ are the in-plane strains under composite action.

Substituting Equation 7 into Equation 6 yields:

$$(8)\quad \frac{\Delta C}{C_0} = (1 + \varepsilon_{x,c})^2(1 - \nu_{xy,c} * \varepsilon_{x,c})^2 - 1$$

SYNTHETIC MEASUREMENTS THROUGH FEM

Synthetic cSEC measurements are produced through FEM simulations by computing local changes in the sensor geometry. Suppose the sensor is meshed using a total of P tetrahedrons (Figure 2b) with each tetrahedron subdivided into Q cuboids (Figure 2a). The capacitance of each mesh element can be written as:

$$(9)\quad \frac{\Delta C^{p,q}}{C_0^{p,q}} = \left(1 + \varepsilon_{xy,c}^{p,q}\right)^2 - \left(1 - \nu_{xy,c}^{p,q} * \varepsilon_{x,c}^{p,q}\right)^2 - 1 = \frac{A^{p,q}}{A_0^{p,q}}$$

where

the superscript p, q indicates the qth cuboid of the pth mesh element, and

$A^{p,q}$ and $A_0^{p,q}$ represent the deformed and initial area of the pth mesh element, respectively.

By extracting strain deformations over all elements, the capacitance response of a synthetic cSEC can be obtained by summing the capacitance of each mesh element and expressed as:

$$(10)\quad \frac{\Delta C}{C_0} = \frac{1}{p \cdot q}\sum_{p=1}^{P}\sum_{q=1}^{Q}\frac{\Delta C^{p,q}}{C_0^{p,q}}$$

Methodology

This section presents the methodology used for the experimental tests and the numerical simulation.

Experimental Test

To experimentally characterize the capacitance response of the cSEC on monitoring angular motion, a free rotational hinge was used to generate angular rotations. The schematic and dimensions of the free rotational hinge equipped with a cSEC are shown in Figure 2b. It consists of two identical panels printed by a fused fitment fabrication 3D printer. The free

rotational hinge was assembled by press-fitting a copper rod into the designed hole, forming a pin connecting both panels and allowing a 90° rotation in both clockwise (CW) and counterclockwise (CCW) directions.

Figures 3a and 3b present the experimental setup. A grid-patterned corrugation for the sensor was selected in this study for ease of fabrication. The free rotational hinge was initially rotated to a flat surface in the *x*-*y* plane (taken as 0°), and the cSEC was adhered onto the *x*-*y* plane spanning the hinge symmetrically using a thin layer of an off-the-shelf bi-component epoxy. The bottom inset of Figure 3b shows a photograph of the installed sensor. Approximately 2% pre-stretching was applied to the cSEC during the installation to prevent any slack or warping of the sensor under rotation-induced compressive strain. Quality of the adhesion process can be evaluated by measuring the initial capacitance of the sensor after installation, where it is expected to be 0.3 to 0.5 pF higher than the initial value before the applied pre-strain. The entire specimen was mounted onto a customized woodblock assembled with two M6 × 1.0 in. stainless coarse thread carriage bolts used to applied strain through controllable displacement (1 mm/cycle). The two edges of the hinge plates were fixed to the woodblock using double-coated urethane foam tape to restrain lateral movement. Displacements of 0, 0.54, 0.22, 0.49, 0.86, 1.34, 1.91, 2.57, 3.31, 4.12, and 5.00 mm were applied on the hinge to induce angles of rotation ($\Delta\alpha$) of 0°, 6°, 12°, 18°, 24°, 30°, 36°, 42°, 48°, 54°, and 60°. Those angular rotations were measured using a digital angle gauge with a minimum resolution of 0.05°, as shown in Figure 3c. This procedure was repeated three times and capacitance data were continuously collected over 120 s at 10 samples/s using an off-the-shelf data acquisition system under each angle.

Numerical Simulations

To validate results obtained from the experimental tests and further validate the cSEC, a nonlinear 3D FEM was constructed in ANSYS release 19.1 (ANSYS 2021) to simulate the capacitance response of the cSEC under nonuniform bending strain. The configuration of the numerical model was created to be identical to the hinge specimen used in the experiments to reproduce tests. The boundary conditions of the numerical model are shown in the inset of Figures 3d and 3e. The rotated angles were labeled as $\Delta\alpha$ and $\Delta\beta$ for rotations in the CW and CCW directions, respectively. Figure 3g presents the simulated deformation of the SEC sensor under a 12° CW direction ($\Delta\alpha$ = 12) angular rotation-induced bending, with the front section view shown in Figure 3g. It can be observed that the deformation field under the sensing area is nonuniform and that the majority

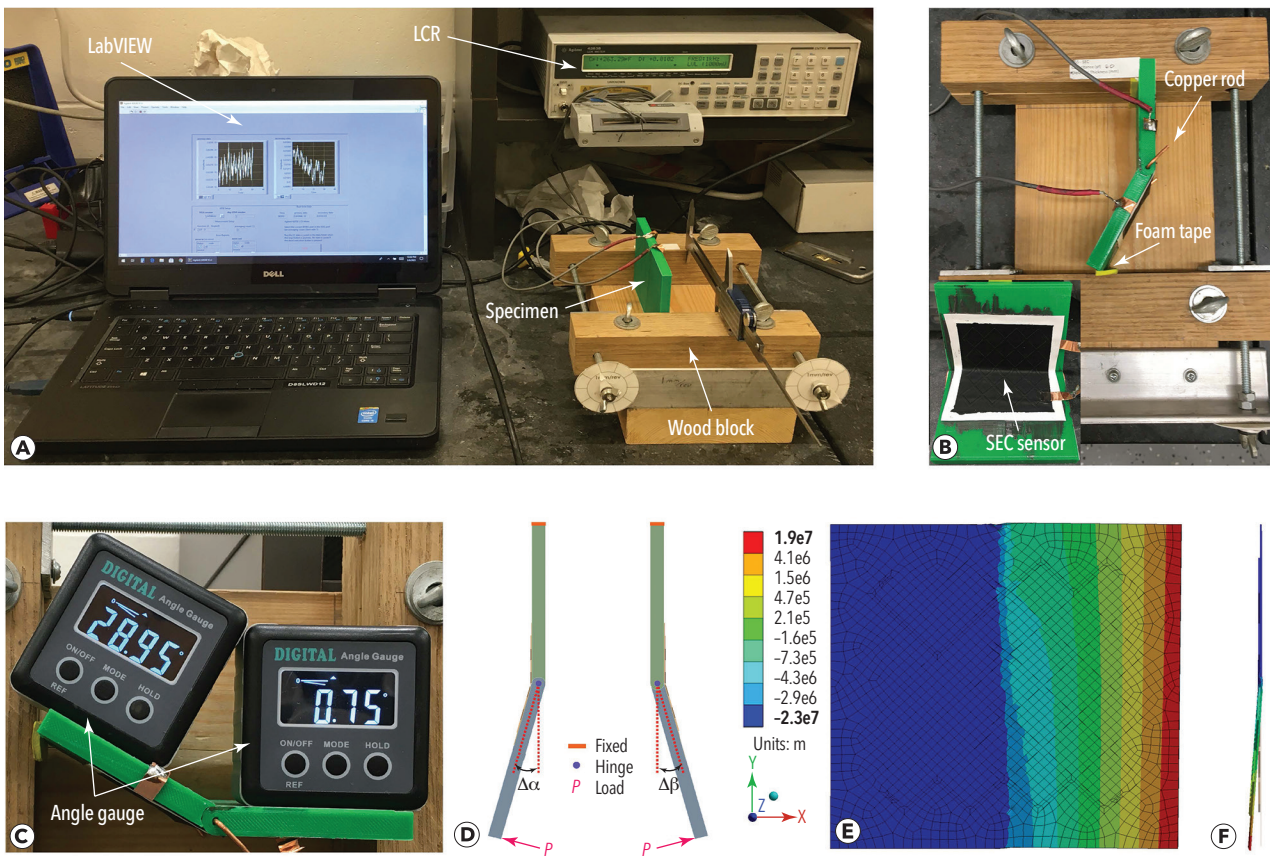

Figure 3. Experimental setup: (a) overview; (b) close-up view of the free rotational hinge; (c) installed digital angle gauges; (d) boundary conditions of the numerical model; (e) simulated deformation of the SEC sensor under a 12° CW rotation; (f) front section view of the deformed sensor under angular motion.

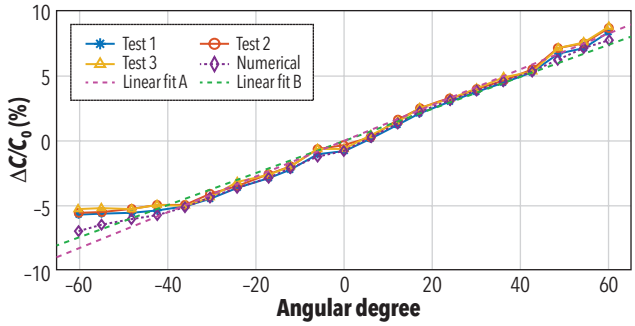

Figure 4. $\Delta C/C_0$ amplitudes as a function of rotated angular degree.

of deformations are localized on the rotated panel, gradually descending from the hinge to the edge of the sensor.

Results and Discussion

The cSEC signal under angular motion was investigated by evaluating the relative change in capacitance $\Delta C/C_0$ under various angular degrees of rotation. Figure 4a is a plot of $\Delta C/C_0$ as a function of the angular rotation in both CW and CCW directions.

Results of the $\Delta C/C_0$ are presented as the averaged values taken from 120 s measurements under each angle. Figure 4 also compares experimental results with those obtained from the numerical simulations. The numerical capacitance response was obtained by extracting elastic strain deformations of each mesh element on the sensor from the FEM and substituting them into Equation 10. Results are shown by the dotted line. A good match is observed between the experimental and numerical data, with a root mean square error (RMSE) remaining constant in the ranges of 3.1% to 5.8% and 3.4% to 7.1% in the CW and CCW directions, respectively. Overall, an approximate linear relationship can be observed from –60° to 60° and the measurements are verified to be repeatable by showing an overlap of the experimental data obtained from three tests, which demonstrates the capability of the cSEC for monitoring static angular deformations.

Figure 4 also shows two linear fits to evaluate the linearity of the sensor. The first linear fit (linear fit A) is conducted over the entire set of data, yielding an R^2 value of 0.92. A poor fit can be observed over the range of –60° to –40°, attributable to the slack in the sensor under large compressive deformations (in the CCW direction). Such slack can be minimized by applying larger prestrain during the sensor installation process. The second linear fit (linear fit B) is conducted over the range –40° to 60°, with an R^2 value of 0.98, showing that the sensor exhibits good linearity over that range. We hypothesize that the sensor would exhibit good linearity beyond 60° until the localized deformation reaches 40% strain (Liu, H. et al. 2020b). Under this specific configuration, the study of the sensor's linearity is limited in compression for angles of rotation greater than 40°.

Conclusion

This paper presented a study investigating the performance of a flexible and compliant strain gauge termed corrugated soft elastomeric capacitor (cSEC) for measuring large angular motions. The sensor is a thin-film capacitor that transduces strain induced by angular motion into a measurable change in capacitance. An electromechanical model was derived to transform capacitance measurements into angular motion, and a finite element model (FEM) was constructed to validate experimental results.

The study was conducted by adhering cSECs onto the rotating area of a free rotational hinge subjected to an axial displacement generating CW and CCW angular rotations between –60° and 60° from a flat surface. Results show that (1) FEM simulations agreed with experimental data; (2) the cSEC produced a linear response in measurements between –40° and 60°; and (3) measurements were repeatable.

Results presented in this study were obtained under static deformations, showing the promise of the cSEC at being used as an angular rotation sensor. Future work includes the study of the sensor behavior under dynamic motion, improvement of the accuracy on angular rotation measurements, and the evaluation of its capability to detect and measure fatigue cracks in corner welds.

ACKNOWLEDGMENTS

The authors gratefully acknowledge the financial support of the Departments of Transportation of Iowa, Kansas, South Carolina, and North Carolina, through Transportation Pooled Fund Study TPF-5(449), and of the American Society for Nondestructive Testing (ASNT) for the Fellowship Award.

REFERENCES

Algrain, M., and J. Saniie. 1991. "Estimation of 3d angular motion using gyroscopes and linear accelerometers." *IEEE Transactions on Aerospace and Electronic Systems* 27 (6): 910–20. https://doi.org/10.1109/7.104259.

Anandan, N., A. Varma Muppala, and B. George. 2018. "A flexible, planar-coil-based sensor for through-shaft angle sensing." *IEEE Sensors Journal* 18 (24): 10217–24. https://doi.org/10.1109/JSEN.2018.2874065.

ANSYS. 2021. Release 19.1. Academic research mechanical. Commercial research.

Askari, H., E. Asadi, Z. Saadatnia, A. Khajepour, M. B. Khamesee, and J. Zu. 2018. "A flexible tube-based triboelectric–electromagnetic sensor for knee rehabilitation assessment." *Sensors and Actuators. A, Physical* 279:694–704. https://doi.org/10.1016/j.sna.2018.05.016.

Chowdhury, A. R., A. M. Abdullah, I. Hussain, J. Lopez, D. Cantu, S. K. Gupta, Y. Mao, S. Danti, and M. J. Uddin. 2019. "Lithium doped zinc oxide based flexible piezoelectric-triboelectric hybrid nanogenerator." *Nano Energy* 61:327–36. https://doi.org/10.1016/j.nanoen.2019.04.085.

Davidovits, P. 2018. *Physics in Biology and Medicine*. Cambridge, MA: Academic Press.

Gao, W., B. Ma, J. Luo, and J. Deng. 2019. "High sensitive polyimide-based single-walled carbon nanotube thermal film sensor for fluid shear stress measurements." *Smart Materials and Structures* 28 (7): 075021. https://doi.org/10.1088/1361-665X/ab1cc3.

Gowthaman, N., P. Arul, J.-J. Shim, and S. A. John. 2019. "Free-standing au-ag nanoparticles on carbon cloth: A non-enzymatic flexible electrochemical sensor for the biomarker of oxidative stress." *Applied Surface Science* 495:143550. https://doi.org/10.1016/j.apsusc.2019.143550.

Guo, Z., L. Mo, Y. Ding, Q. Zhang, X. Meng, Z. Wu, Y. Chen, M. Cao, W. Wang, and L. Li. 2019. "Printed and flexible capacitive pressure sensor with carbon nanotubes based composite dielectric layer." *Micromachines* 10 (11): 715. https://doi.org/10.3390/mi10110715.

Jiao, Y., C. W. Young, S. Yang, S. Oren, H. Ceylan, S. Kim, K. Gopalakrishnan, P. C. Taylor, and L. Dong. 2016. "Wearable graphene sensors with microfluidic liquid metal wiring for structural health monitoring and human body motion sensing." *IEEE Sensors Journal* 16 (22): 7870–75. https://doi.org/10.1109/JSEN.2016.2608330.

Laflamme, S., H. S. Saleem, B. K. Vasan, R. L. Geiger, D. Chen, M. R. Kessler, and K. Rajan. 2013. "Soft elastomeric capacitor network for strain sensing over large surfaces." *IEEE/ASME Transactions on Mechatronics* 18 (6): 1647–54. https://doi.org/10.1109/TMECH.2013.2283365.

Laflamme, S., F. Ubertini, H. Saleem, A. D'Alessandro, A. Downey, H. Ceylan, and A. L. Materazzi. 2015. "Dynamic characterization of a soft elastomeric capacitor for structural health monitoring." *Journal of Structural Engineering* 141 (8): 04014186. https://doi.org/10.1061/(ASCE)ST.1943-541X.0001151.

Liu, G., Q. Tan, H. Kou, L. Zhang, J. Wang, W. Lv, H. Dong, and J. Xiong. 2018. "A flexible temperature sensor based on reduced graphene oxide for robot skin used in internet of things." *Sensors (Basel)* 18 (5): 1400. https://doi.org/10.3390/s18051400.

Liu, H., M. Kollosche, J. Yan, E. M. Zellner, S. A. Bentil, I. V. Rivero, C. Wiersema, and S. Laflamme. 2020a. "Numerical investigation of auxetic textured soft strain gauge for monitoring animal skin." *Sensors (Basel)* 20 (15): 4185. https://doi.org/10.3390/s20154185.

Liu, H., J. Yan, M. Kollosche, S. A. Bentil, and S. Laflamme. 2020b. "Surface textures for stretchable capacitive strain sensors." *Smart Materials and Structures* 29 (10): 105037. https://doi.org/10.1088/1361-665X/aba63c.

Liu, H., S. Laflamme, J. Li, C. Bennett, W. N. Collins, A. Downey, and H. Jo. 2021a. "Experimental validation of textured sensing skin for fatigue crack monitoring." In *Sensors and Smart Structures Technologies for Civil, Mechanical, and Aerospace Systems 2021*, ed. D. Zonta, H. Huang, and Z. Su. SPIE. https://doi.org/10.1117/12.2582592.

Liu, H., S. Laflamme, J. Li, C. R. Bennett, W. Collins, A. Downey, P. Ziehl, and H. Jo. 2021b. "Investigation of surface textured sensing skin for fatigue crack localization and quantification." *Smart Materials and Structures* 30 (10): 105030. https://doi.org/10.1088/1361-665X/ac221a.

Liu, H., S. Laflamme, E.M. Zellner, A. Aertsens, S. A. Bentil, I. V. Rivero, and T. W. Secord. 2021c. "Soft elastomeric capacitor for strain and stress monitoring on sutured skin tissues." *ACS Sensors* 6 (10): 3706–14. https://doi.org/10.1021/acssensors.1c01477.

Liu, J., D. Yu, Z. Zheng, G. Huangfu, and Y. Guo. 2021. "Lead-free BiFeO3 film on glass fiber fabric: Wearable hybrid piezoelectric-triboelectric nanogenerator." *Ceramics International* 47 (3): 3573–79. https://doi.org/10.1016/j.ceramint.2020.09.205.

Liu, Q., H. Tai, Z. Yuan, Y. Zhou, Y. Su, and Y. Jiang. 2019. "A high-performances flexible temperature sensor composed of polyethyleneimine/reduced graphene oxide bilayer for real-time monitoring." *Advanced Materials Technologies* 4 (3): 1800594. https://doi.org/10.1002/admt.201800594.

Mu, C., Y. Song, W. Huang, A. Ran, R. Sun, W. Xie, and H. Zhang. 2018. "Flexible normal-tangential force sensor with opposite resistance responding for highly sensitive artificial skin." *Advanced Functional Materials* 28 (18): 1707503. https://doi.org/10.1002/adfm.201707503.

Peña Arellano, F.E., H. Panjwani, L. Carbone, and C. C. Speake. 2013. "Interferometric measurement of angular motion." *Review of Scientific Instruments* 84 (4): 043101. https://doi.org/10.1063/1.4795549.

Penning, L., R. Irwan, and M. Oudkerk. 2005. "Measurement of angular and linear segmental lumbar spine flexion-extension motion by means of image registration." *European Spine Journal* 14 (2): 163–70. https://doi.org/10.1007/s00586-004-0761-x.

Prituja, A. V., H. Banerjee, and H. Ren. 2018. "Electromagnetically enhanced soft and flexible bend sensor: A quantitative analysis with different cores." *IEEE Sensors Journal* 18 (9): 3580–89. https://doi.org/10.1109/JSEN.2018.2817211.

Qu, M., Y. Qin, Y. Sun, H. Xu, D. W. Schubert, K. Zheng, W. Xu, and F. Nilsson. 2020. "Biocompatible, flexible strain sensor fabricated with polydopamine-coated nanocomposites of nitrile rubber and carbon black." *ACS Applied Materials & Interfaces* 12 (37): 42140–52. https://doi.org/10.1021/acsami.0c11937.

Shao, L., X. Zhao, S. Gu, Y. Ma, Y. Liu, X. Deng, H. Jiang, and W. Zhang. 2021. "Pt thin-film resistance temperature detector on flexible hastelloy tapes." *Vacuum* 184:109966. https://doi.org/10.1016/j.vacuum.2020.109966.

Sun, X., Z. Qin, L. Ye, H. Zhang, Q. Yu, X. Wu, J. Li, and F. Yao. 2020. "Carbon nanotubes reinforced hydrogel as flexible strain sensor with high stretchability and mechanically toughness." *Chemical Engineering Journal* 382:122832. https://doi.org/10.1016/j.cej.2019.122832.

Tannarana, M., G. K. Solanki, S. A. Bhakhar, K. D. Patel, V. M. Pathak, and P. M. Pataniya. 2020. "2d- SnSe2 nanosheet functionalized piezo-resistive flexible sensor for pressure and human breath monitoring." *ACS Sustainable Chemistry & Engineering* 8 (20): 7741–49. https://doi.org/10.1021/acssuschemeng.0c01827.

Viola, F. A., A. Spanu, P. C. Ricci, A. Bonfiglio, and P. Cosseddu. 2018. "Ultrathin, flexible and multimodal tactile sensors based on organic field-effect transistors." *Scientific Reports* 8 (1): 8073. doi:10.1038/s41598-018-26263-1.

Wang, X., M. Wei, X. Li, S. Shao, Y. Ren, W. Xu, M. Li, W. Liu, X. Liu, and J. Zhao. 2020. "Large-area flexible printed thin-film transistors with semiconducting single-walled carbon nanotubes for NO2 sensors." *ACS Applied Materials & Interfaces* 12 (46): 51797–807. https://doi.org/10.1021/acsami.0c13824.

Yang, X., Y. Wang, and X. Qing. 2019. "A flexible capacitive sensor based on the electrospun PVDF nanofiber membrane with carbon nanotubes." *Sensors and Actuators. A, Physical* 299:111579. https://doi.org/10.1016/j.sna.2019.111579.

Yu, Z., G. Cai, X. Liu, and D. Tang. 2021. "Pressure-based biosensor integrated with a flexible pressure sensor and an electrochromic device for visual detection." *Analytical Chemistry* 93 (5): 2916–25. https://doi.org/10.1021/acs.analchem.0c04501.

Zhang, J.-h., and C.-H. Menq. 1999. "A linear/angular interferometer capable of measuring large angular motion." *Measurement Science and Technology* 10 (12): 1247–1253. https://doi.org/10.1088/0957-0233/10/12/317.